Xiaofeng Guo, Xiaoxiang Weng, Yong Jiang and Jianming Gong*

Effects of Temperature and Strain Rate on Tensile Deformation Behavior of 9Cr-0.5Mo-1.8W-VNb Ferritic Heat-Resistant Steel

DOI 10.1515/htmp-2016-0065
Received March 27, 2016; accepted August 22, 2016

Abstract: A series of uniaxial tensile tests were carried out at different strain rate and different temperatures to investigate the effects of temperature and strain rate on tensile deformation behavior of P92 steel. In the temperature range of 30–700 °C, the variations of flow stress, average work-hardening rate, tensile strength and ductility with temperature all show three temperature regimes. At intermediate temperature, the material exhibited the serrated flow behavior, the peak in flow stress, the maximum in average work-hardening rate, and the abnormal variations in tensile strength and ductility indicates the occurrence of DSA, whereas the sharp decrease in flow stress, average work-hardening rate as well as strength values, and the remarkable increase in ductility values with increasing temperature from 450 to 700 °C imply that dynamic recovery plays a dominant role in this regime. Additionally, for the temperature ranging from 550 to 650 °C, a significant decrease in flow stress values is observed with decreasing in strain rate. This phenomenon suggests the strain rate has a strong influence on flow stress. Based on the experimental results above, an Arrhenius-type constitutive equation is proposed to predict the flow stress.

Keywords: P92 steel, tensile tests, dynamic strain aging

Introduction

Recently, the growing demand of energy conservation and environmental protection has driven the development of the new generation nuclear power technology. As one of the most promising fission nuclear reactors in generation IV nuclear power plant, super-critical water-cooled reactor (SCWR) is proposed by several countries [1, 2]. For this next generation nuclear reactor, the structural material operating at high temperature under service stress needs to have excellent mechanical properties, oxidation resistance and irradiation resistance [3]. ASME grade 92 steel (9Cr-0.5Mo-1.8W-VNb) previously developed for ultra-supercritical power plants has been recognized as one of the candidates for the structural components of the new generation nuclear reactors, such as reactor vessels and pipes [4, 5].

In the past decades, a series of studies have been carried out to investigate the effect of temperature and stress on the mechanical properties, creep, low-cycle fatigue, and creep-fatigue behavior of T/P92 steel [6–14], and large amounts of data are available. Compared with the service temperature of ultra-supercritical power plants, this material used for SCWR exposes to lower temperature, but the service environment is more complex due to the irradiation. Meanwhile, several studies have found that T/P91 steel exhibits serrated flow behavior at intermediate temperature (250–450 °C) which indicates the occurrence of Portevin-Le Chatelier (PLC) effect [15, 16]. As is well-known, this effect gives rise to the degradation of mechanical properties, such as reduction in fracture toughness, the loss of ductility and decrease in fatigue life. Because T/P92 steel is developed from T/P91 steel by a reduction of Mo from 1 to 0.5 % and an addition of 1.8 %W, it is necessary to study the PLC effect of T/P92 steel due to plastic instability during the plastic deformation at intermediate temperature. At present, few attempts have been concentrated on the effect of temperature and strain rate on the tensile deformation behavior of P92 steel. Additionally, the PLC effect of P92 steel has not been fully understood.

Therefore, a series of uniaxial tensile tests were carried out to systematically investigate the influence of temperature and strain rate on the tensile properties of P92 steel. Moreover, the micro-mechanism of the occurrence of PLC effect was discussed in the following section. Based on the experimental results above, an Arrhenius-type constitutive equation was proposed.

***Corresponding author: Jianming Gong,** School of Mechanical and Power Engineering, Nanjing Tech University, Nanjing, Jiangsu 210009, China, E-mail: gongjm@njtech.edu.cn
Xiaofeng Guo, School of Mechanical and Power Engineering, Nanjing Tech University, Nanjing, Jiangsu 210009, China; School of Mechanical Engineering, Inner Mongolia University of Science and Technology, Baotou, Inner Mongolia 014010 China
Xiaoxiang Weng, Yong Jiang, School of Mechanical and Power Engineering, Nanjing Tech University, Nanjing, Jiangsu 210009, China

Experimental procedures

The P92 steel, 390 mm diameter, 70 mm wall thickness pipe, was investigated in the study. The pipe was normalized at 1,070 °C, followed by tempering at 760 °C. The chemical composition of the material is shown in Table 1. The tensile specimens were machined from the pipe along longitudinal axial direction. The gauge length and diameter of the standard push-pull cylindrical specimens were 30 mm and 5 mm.

All the tensile tests were performed with an INSTRON 5869 vertical tensile testing machine equipped with a three-zone temperature control furnace. The temperatures in all the tests were controlled within ± 1 °C. In order to investigate the effect of temperature on the tensile properties of P92 steel, a series of tensile tests were performed over a temperature range of 30–700 °C at the strain rate of 5×10^{-5} s^{-1}. Furthermore, some tensile tests were carried out at high temperature (550–650 °C) in the strain rate range of 1×10^{-5} s^{-1} to 1×10^{-3} s^{-1}. During the tests, 0.2% proof stress (σ_{ys}) and Young's modulus value (E) were measured when the specimens were pulled to the strain level of 1% in the first phase controlled by strain mode. This initial strain rate was controlled by an extensometer. In the second phase, these specimens controlled by displacement mode were pulled up to fracture to determine the ultimate tensile strength (σ_{ult}) and the elongation (δ). Meanwhile, the stress–strain plots were recorded continuously in a computer.

A transmission electron microscopy (TEM) sample was examined to reveal the typical microstructure in the initial state using JEOL JEM-2010. This sample was first mechanically thinned to 0.1 mm, and then thinned down to 60 μm or less using emery paper before further thinning using GATAN PIPS-691.

Results and discussion

Microstructure of as-received material

Figure 1 shows TEM images of the initial state of P92 steel. It can be seen in Figure 1(a) that the steel exhibits a pronounced tempered martensitic matrix which is composed of some elements at several scales: prior austenite grains, packet of blocks, block of laths, martensitic laths and subgrains. In addition, these boundaries and subgrain boundaries are decorated by $M_{23}C_6$ carbide precipitated mainly along prior austenite grain boundaries and subgrain boundaries and MX carbonitrides distributed in grain interior; the initial dislocation density inside the subgrains is very high, as shown in Figure 1(b).

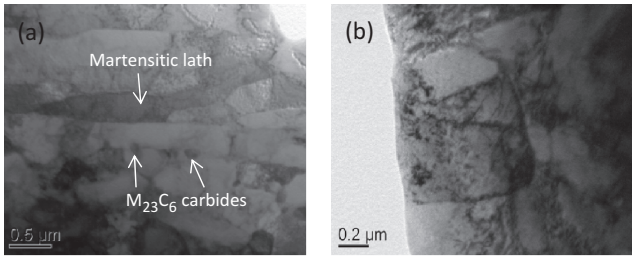

Figure 1: TEM micrographs of the initial state of P92 steel: (a) the pronounced tempered martensitic matrix and (b) high density of dislocation.

Effect of temperature on tensile stress–strain behavior

The engineering stress–strain curves

The engineering stress–strain curves of P92 steel at the strain rate of 5×10^{-5} s^{-1} at the temperature in the range of 30–700 °C are investigated in the present study, and some serrations are observed on the stress–strain plot. Figure 2 represents the typical segments of stress–strain curves exhibited in arbitrary unit at the strain rate of 5×10^{-5} s^{-1} for the temperature ranging from 200 to 400 °C. As one of the most important characteristics, the emergence of serrated flow indicates the occurrence of PLC effect. At present, it is widely accepted that the physical origin of this effect is attributed to dynamic strain aging (DSA). Given the scattering of the force measurement, stress oscillations under 5 MPa are not regarded as DSA serrations. Based on the criterion, the critical temperature for the onset of DSA is identified to be around 250 °C, whereas DSA serrations are not

Table 1: Chemical composition (wt%) of the steel studied.

C	Mn	P	S	Si	Cr	W	Mo	V	Nb	N	B	Ni	Al
0.114	0.392	0.011	0.004	0.315	9.21	1.93	0.475	0.189	0.073	0.037	0.003	0.275	0.011

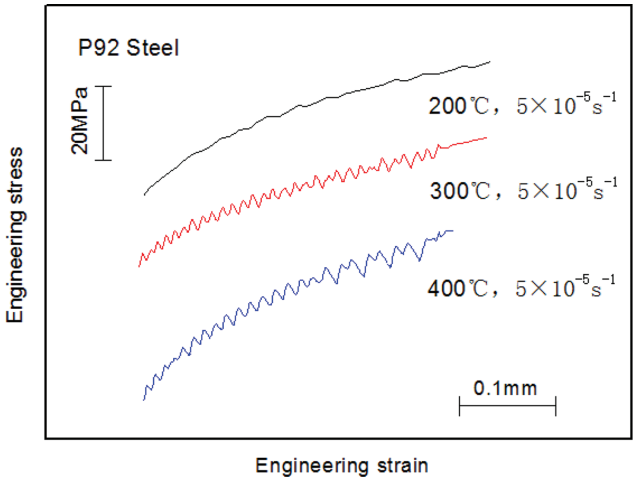

Figure 2: Segments of engineering stress–strain curves of P92 steel obtained from tensile tests at three different temperatures at the strain rate of 5×10^{-5} s^{-1}.

noticed at 30 °C and 200 °C. Moreover, the intensity of serrations increases with increasing temperature ranging from 250 to 450 °C. For this temperature range, it is obvious that the intensity of serrations is found to be strongly dependent on temperature which is manifested by the height of serrations, as seen in Figure 2. The magnitude of the stress drop increases with increasing temperature. This phenomenon could be explained by DSA. As reported by many researchers [17–19], DSA is governed by the dragging of solute atoms at the mobile dislocation which is arrested by the obstacles, such as forest dislocation and grain boundaries. Due to the increase of the friction stress caused by the dragging of solute atoms, the mobile dislocation is pinned by the solute atoms. However, when the tensile stress increases, owing to the increase of the velocity of mobile dislocation, the atmosphere of solute atoms is peeled off from mobile dislocation. Then, the tensile stress is decreased because of the reduction of the friction stress. Meanwhile, the dislocation velocity is decreased by the reduction of the tensile stress. So the solute atmosphere is formed again around dislocation which is pinned by the solute atoms. This cyclically dragging of solute atoms process induces the serration on the stress–strain curves. It is well-known that the diffusion of solute atoms can be accelerated by the increase of the temperature which leads to larger numbers of solute atoms to diffuse to the dislocation. It increases the strength of solute locking with increasing temperature. So the intensity of serrations increases with increase of the temperature ranging from 250 to 450 °C. When the temperature exceeds 450 °C, the serration amplitude reduces gradually. This indicates the progressive disappearance of the DSA, and the occurrence of dynamic recovery at high temperature.

The variation of flow stress with temperature

Figure 3 shows the typical true stress (σ_t) – true plastic strain (ε_p) curves of P92 steel at strain rate of 5×10^{-5} s^{-1} in the temperature range of 30–700 °C, which is expressed in the double logarithmic plots. From all the curves above, it is worth noting that σ_t–ε_p curves fall into a very narrow band at low and intermediate temperature in the range of 30–450 °C, and then a rapid decrease in stress values is observed with increase of the temperature over 500 °C. This result is similar to the findings investigated by Kimura et al. [20].

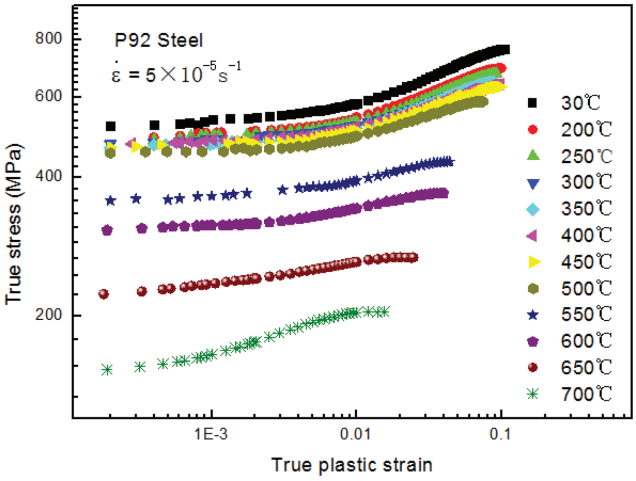

Figure 3: True stress–true plastic strain curves of P92 steel at strain rate of 5×10^{-5} s^{-1}.

In order to understand the variation of flow stress with temperature, normalized flow stress versus temperature plot at different plastic strain, such as 0.001, 0.002, 0.005, 0.01, 0.02 and 0.05, is presented in Figure 4, where temperature-dependent Young's modulus value (E) is used in this normalized procedure. It is visible from Figure 4 that there are three pronounced temperature regimes. For the temperature ranging from 30 to 200 °C, the normalized flow stress displays a slight decrease in regime I. As is well-known, the plastic deformation of the steel is linked to the motion of the dislocation. At low temperature, the motion of the dislocation is quite difficult, due to a large friction stress by reason of the Peierls valley. However, this friction stress can be overcome by increasing temperature. Thus, a marginal

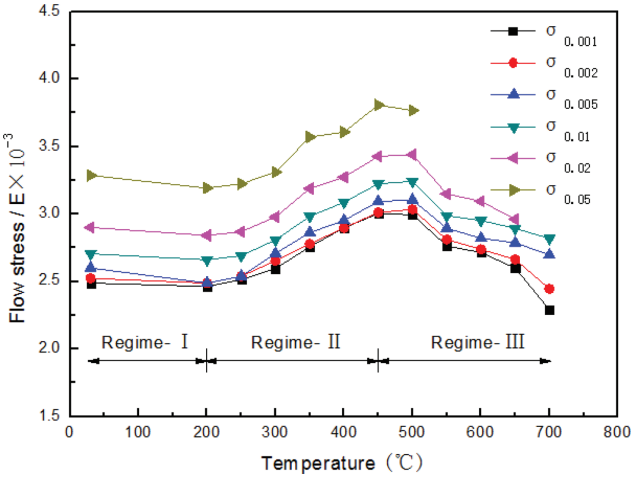

Figure 4: Variations of normalized flow stress at different true plastic strain with temperature at strain rate of 5×10^{-5} s^{-1}.

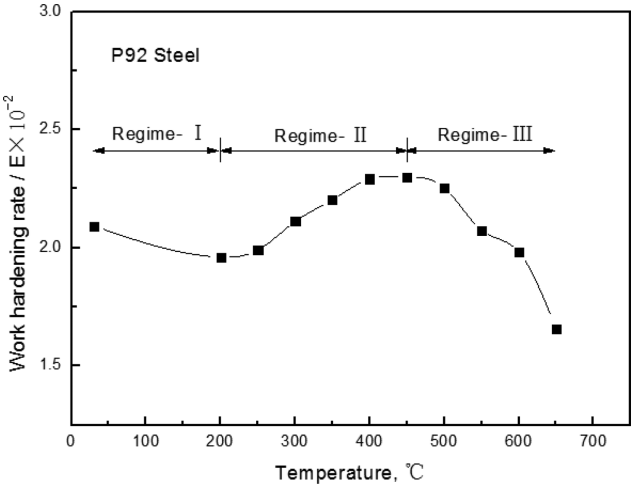

Figure 5: Variations of normalized average work-hardening rate with temperature at strain rate of 5×10^{-5} s^{-1}.

decrease in flow stress is observed for this temperature range. In regime II, a stress peak is observed at intermediate temperature, and this abnormal phenomenon could be explained by DSA. It has been demonstrated above the dragging of solute atoms hinders the motion of the mobile dislocation which is temporarily arrested by the obstacles. In this regime, the increasing temperature promotes faster diffusion of solute atoms, so the additional pinning effect is produced. This results in a larger solute atmosphere around the dislocation which delays in the recovery of dislocation. Meanwhile, owing to the dislocation pile-up and tangling, dislocation annihilation rate decreases with increasing temperature from 250 to 450 °C. Therefore, the increase of flow stress is observed in this regime. In regime III, a rapid decrease in flow stress is observed with increasing temperature in the range of 500–700 °C. It indicates the dynamic recovery taking place at high temperature. This dynamic recovery is associated with the decrease in dislocation density, and formation of well-defined dislocation subgrain with increasing temperature [21].

The effect of temperature on average work-hardening rate

Figure 5 shows the variation of normalized average work-hardening rate (θ_a) with respect to temperature at strain rate of 5×10^{-5} s^{-1}. Here, the average work-hardening rate is calculated as:

$$\theta_a = \frac{\sigma_{0.02} - \sigma_{0.002}}{0.018} \quad (1)$$

where $\sigma_{0.002}$ and $\sigma_{0.02}$ are true plastic stress at true plastic strain of 0.002 and 0.02, respectively. Just as the variation of flow stress with respect to temperature, the effect of temperature on the average work-hardening rate also exhibits three temperature regimes. A slight decrease in the normalized average work-hardening rate is observed in regime I followed by the continuous rise with increasing temperature from 250 to 450 °C. Then, the normalized average work-hardening rate values decrease significantly when the temperature exceeds 500 °C. Generally speaking, the normalized average work-hardening rate decreases with the increase of the temperature due to the increase of the recovery with increasing temperature. So $\theta_a - T$ data show a marginal decrease at low temperature. At intermediate temperature, because of the occurrence of DSA, or more precisely, the interaction between the solute atoms and the dislocation, it enhances the average work-hardening rate of the material. Therefore, the upward trend in the normalized average work-hardening rate occurs within the DSA regime, and the value of the average work-hardening rate reaches the maximum. At high temperature, $\theta_a - T$ curve shows a significant decrease with increasing temperature from 500 °C, and it implies that the dynamic recovery plays a dominant role in this regime.

The variation of tensile properties with temperature

The influence of temperature on normalized yield strength and ultimate tensile strength is shown in Figure 6(a). It can be seen that the variations of yield

strength and ultimate tensile strength with temperature are also composed of three temperature regimes. A decrease in normalized yield strength and ultimate tensile strength is observed with increase of the temperature in the range of 30–200 °C in regime I followed by a continuous increase at intermediate temperature in regime II (250–450 °C). In regime II, it gives rise to a peak value with increase of the temperature, which confirms the occurrence of DSA in this material. At intermediate temperature, the observed normalized yield strength and ultimate tensile strength increase with increasing temperature from 250 to 450 °C, which reflects an increase in the deformation resistance in the DSA temperature regimes. The increase is attributed to enhancing of the diffusion of solute atoms with increasing temperature in the DSA regime. So the solute atoms have sufficient mobility to pin the dislocation, and it results in the trend of the increase of DSA and the reduction of dynamic recovery. However, the normalized yield strength and ultimate tensile strength decrease rapidly at high temperature in regime III (500–700 °C), it suggests that dynamic recovery plays a vital role in this regime.

Compared with the regular variation of yield strength and ultimate tensile strength with temperature, the variation of elongation to fracture (δ) and reduction of area (φ) do not exhibit a good consistency, as shown in Figure 6(b) and (c). The experimental data of both parameters have a certain degree of fluctuation, which may be due to the experimental measurement errors. A general δ–T curve or φ–T curve is comprised of three temperature regimes, where the literature data is also exhibited in order to compare with each other [20, 21]. The variation of elongation to fracture with temperature exhibits a significant decrease with increasing temperature in the range of 30–200 °C in regime I, whereas reduction of area shows a small decrease in this regime. In regime II, there is a slight decrease in elongation to fracture and reduction of area with increase of the temperature in the range of 250–450 °C, and a pronounced increase is noticed at high temperature (500–700 °C) in regime III. It is worth noting that this material shows

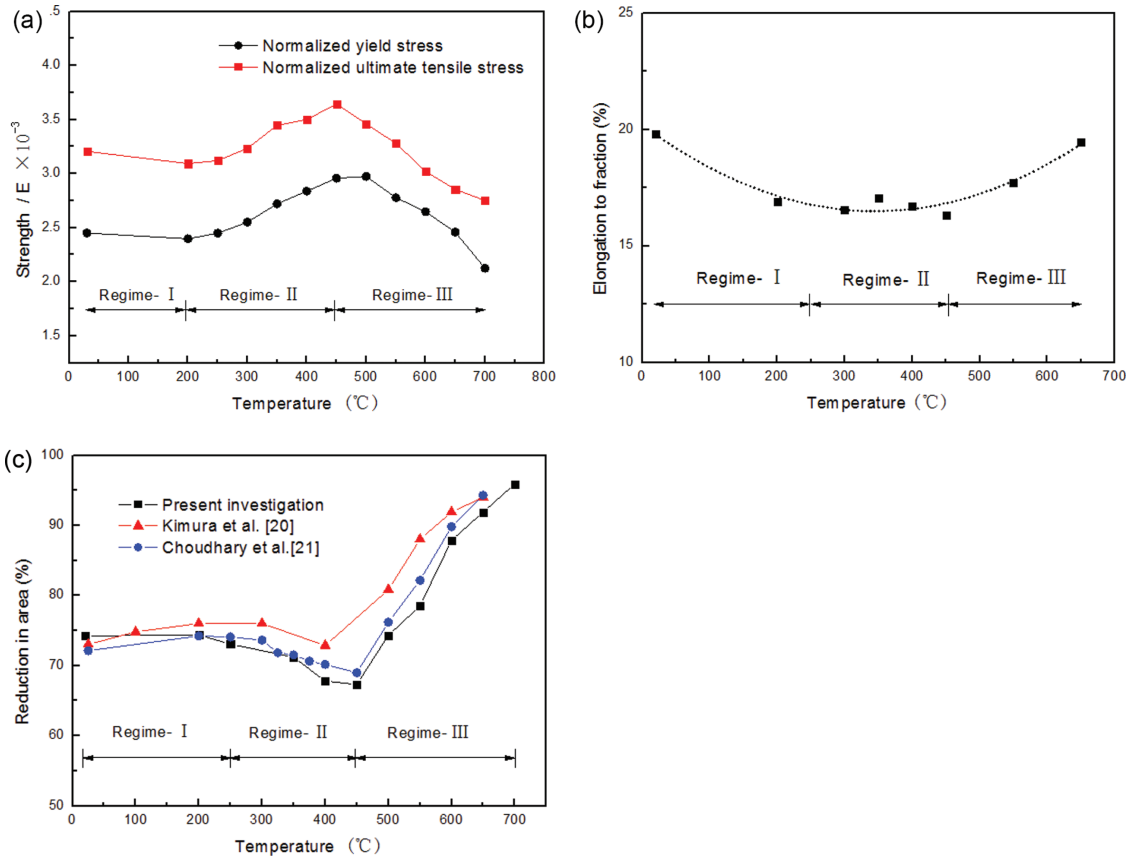

Figure 6: Variations of tensile properties with temperature: (a) normalized yield stress and normalized ultimate tensile stress; (b) elongation; (c) reduction in area.

lower ductility in regime II, compared with regime I(low temperature) and regime III (high temperature). At intermediate temperature, the ductility decreases to the minimum.

The strain sensitivity of P92 steel at high temperature

Figure 7 shows the typical true stress (σ_t) – true plastic strain (ε_p) curves of P92 steel at different strain rate (1×10^{-5} s^{-1} to 1×10^{-3} s^{-1}) in the temperature range of 550–650 °C. It can be seen from Figure 7 the flow stress of P92 steel exhibits strong sensitivity to temperature, strain rate and strain, which can be attributed to the thermal softening, strain rate hardening and strain hardening. It is worth noting that the strain rate sensitivity of P92 steel is obvious at all the temperatures. Moreover, a significant decrease in flow stress values is observed with decreasing in strain rate.

The constitutive equation

In order to understand the effects of temperature and strain rate on flow stress in P92 steel, the constitutive equation is used to define the flow stress as a function of temperature and strain rate. The most widely used constitutive equation can be expressed as:

$$\dot{\varepsilon} = A[\sinh(\alpha\sigma)]^n \exp(-Q/RT) \tag{2}$$

where $\dot{\varepsilon}$ is the strain rate (s^{-1}), σ is the flow stress (MPa), Q is deformation activation energy (KJ/mol), R is the gas constant (J/(mol K)), T is the absolute deformation temperature (K), A, α, n are material constants.

Taking logarithms on both sides of eq. (2) gives

$$\ln\ \dot{\varepsilon} = \ln\ A + n\ln\ [\sinh\ (\alpha\sigma)] - Q/RT \tag{3}$$

From eq. (3), the stress exponent n is defined by

$$n = \frac{\partial \ln \dot{\varepsilon}}{\partial \ln[\sinh(\alpha\sigma)]} \tag{4}$$

Hence, the stress exponent n is determined by the slope coefficients of $\ln\dot{\varepsilon}$ versus $\ln[\sinh(\alpha\sigma)]$. Taking strain = 0.1 % as an example, n can be calculated from Figure 8(a). And the constant α can also be obtained by the slope coefficients of $\ln\dot{\varepsilon}$ versus σ and $\ln\dot{\varepsilon}$ versus $\ln\sigma$, as shown in Figure 8(b) and (c).

The activation energy Q can be expressed as:

$$Q = nR\frac{\partial \ln[\sinh(\alpha\sigma)]}{\partial(1/T)} \tag{5}$$

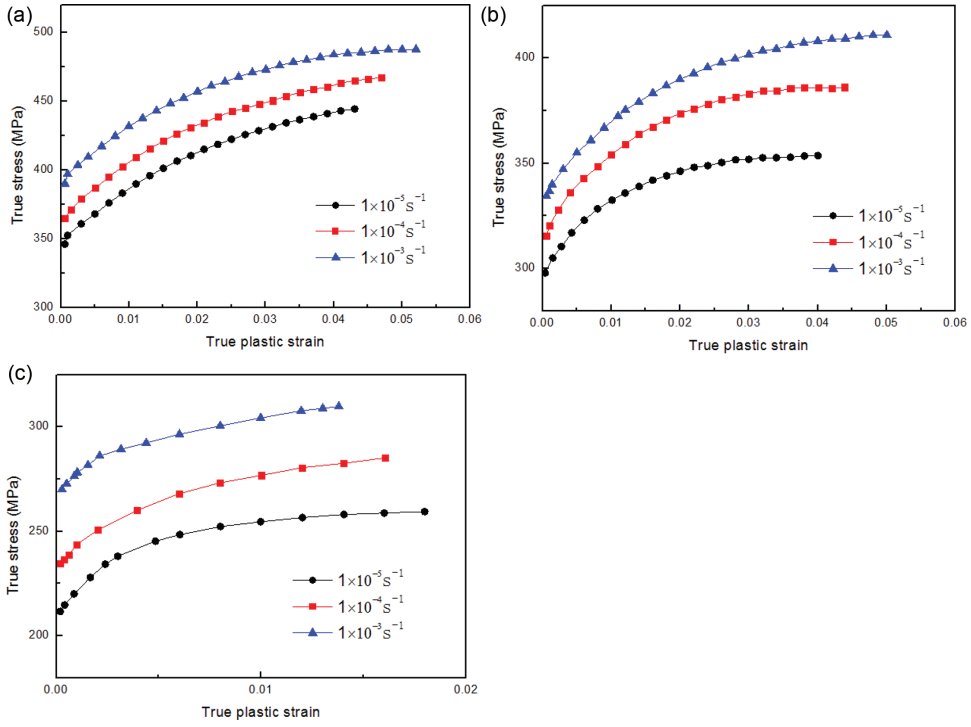

Figure 7: True stress–true plastic strain curves of P92 steel obtained from tensile tests at different strain rate and temperatures of (a) 550 °C; (b) 600 °C; (c) 650 °C.

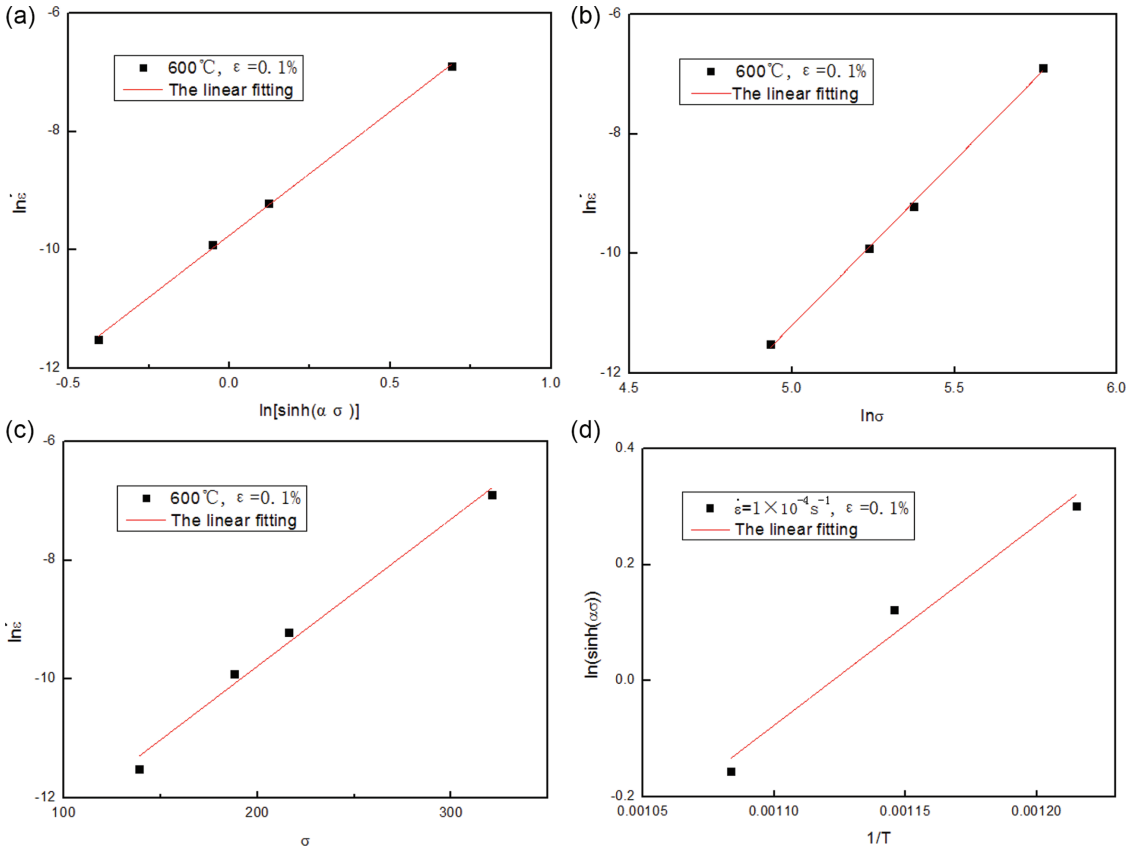

Figure 8: Plots used for calculation of (a) n, (b) and (c) α, (d) Q values.

Thus, the activation energy Q can be determined by slope of ln[sinh($\alpha\sigma$)] versus (1/T) plot, as exhibited in Figure 8(d). Meanwhile, ln$A$ is 0.41 by calculation through the linear extrapolation method. Therefore, the constitutive equation can be written as:

$$\dot{\varepsilon} = 1.51[\sinh(4.34\times10^{-3}\sigma)]^{4.3}\exp(-9.224\times10^{4}/RT) \quad (6)$$

In this constitutive equation, it is worth noting that the value of stress exponent (n) and activation energy (Q) may be relatively small compared with that in other investigations [7, 22]. This result may result from the different manufacturing technology between the thick-walled pipe with large diameter and thin-walled tube with small diameter. In the present study, a pipe with the diameter of 390 mm and the thickness of 70 mm was used for the tests, whereas other investigations commonly used thin-walled tubes. Due to the difficulty of manufacturing technology of thick-walled pipes, there are some differences between the experimental results. In addition, because the experimental material comes from different manufacturers with various chemical compositions and heat treatment procedures, all the factors may also result in these differences between the experimental parameters.

Figure 9 shows the comparison of the predicted and experimental values of $\sigma_{\varepsilon=0.1\%}$ at high temperature (550–650 °C) in the strain rate range of 1×10^{-5} s^{-1} to

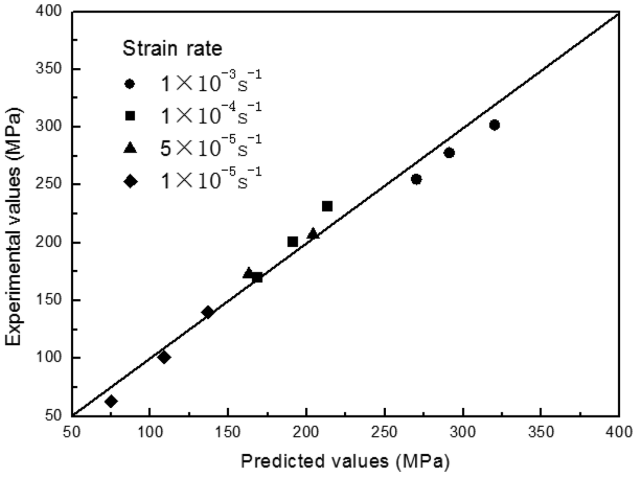

Figure 9: Comparison of the predicted values and the experimental values of $\sigma_{\varepsilon=0.1\%}$ at different strain rate.

1×10^{-3} s^{-1}. It is observed that the predicted values are agreement with the experimental values.

Conclusions

A series of tensile tests were carried out at different strain rate and different temperatures to investigate the effects of temperature and strain rate on tensile deformation behavior of P92 steel. Additionally, an Arrhenius-type constitutive equation is proposed to understand the influence of temperature and strain rate on flow stress in P92 steel. Based on the experimental results above, the main conclusions are as follows:

1. In the temperature range of 30–700 °C, the variations of flow stress, average work-hardening rate, tensile strength and ductility with temperature all exhibit three temperature regimes.
2. At intermediate temperature, the material exhibited the serrated flow behavior, the peak in flow stress, the maximum in average work-hardening rate, and the abnormal variations in tensile strength and ductility indicates the occurrence of DSA. These phenomena are attributed to the interaction between the solute atoms and the dislocation in the DSA regime. At high temperature, the sharp decrease in flow stress, the average work-hardening rate and strength values, and the remarkable increase in ductility values with increasing temperature from 450 to 700 °C imply that dynamic recovery plays a dominant role in this regime.
3. The strain rate sensitivity of P92 steel is obvious in the temperature range of 550–650 °C. Moreover, a significant decrease in flow stress values is observed with decreasing in strain rate.
4. An Arrhenius-type constitutive equation is proposed to predict the flow stress as a function of temperature and strain rate. The result shows that the predicted values are consistent with the experimental values.

Funding: The authors gratefully acknowledge the support provided by the innovation program for graduate students in JiangSu Province of China (No. KYLX15_0800) and the innovation foundation of Inner Mongolia University of Science and Technology (No. 2014QDL023).

References

[1] P. Saha, N. Aksan, J. Andersen, J. Yan, J.P. Simoneau, L. Leung, F. Bertrand, K. Aoto and H. Kamide, Nucl. Eng. Des., 264 (2013) 3–23.
[2] S.E. Langton, A. Buijs and J. Pencer, Ann. Nucl. Energy, 75 (2015) 635–644.
[3] R.W. Grimes, R.J.M. Konings and L. Edwards, Nature Mater., 7 (2008) 683–685.
[4] S.X. Jin, L.P. Guo, T.C. Li, J.H. Chen, Z. Yang, F.F. Lu, R. Tang, Y.X. Qiao and F.H. Liu, Mater. Charact., 68 (2012) 63–70.
[5] T. Abram and S. Ion, Energy Policy, 36 (2008) 4323–4330.
[6] P.F. Giroux, F. Dalle, M. Sauzay, J. Malaplate, B. Fournier and A.F.G. Lorenzon, Mater. Sci. Eng. A, 527 (2010) 3984–3993.
[7] S. Alsagabi, T. Shrestha and I. Charit, J. Nucl. Mater., 453 (2014) 151–157.
[8] J.S. Lee, H.G. Armaki and K. Maruyama, Mater. Sci. Eng. A, 428 (2006) 270–275.
[9] F. Abe, Curr. Opin. Solid State Mater. Sci., 8 (2004) 305–311.
[10] F. Abe, T. Horiuchi, M. Taneike and K. Sawada, Mater. Sci. Eng. A, 378 (2004) 299–303.
[11] V. Sklenicka, K. Kucharova, M. Svoboda, L. Kloc, J. Bursik and A. Kroupa, Mater. Charact., 51 (2003) 35–48.
[12] B. Fournier, F. Dalle, M. Sauzay, J. Longour, M. Salvi, C. Caës, I. Tournié, P.F. Giroux and S.H. Kim, Mater. Sci. Eng. A, 528 (2011) 6934–6945.
[13] K.X. Shi, F.S. Lin, H.B. Wan and Y.F. Wang, Mater. High Temp., 31 (2014) 343–347.
[14] B. Fournier, M. Salvi, F. Dalle, Y.D. Carlan, C. Caës, M. Sauzay and A. Pineau, Int. J. Fatigue, 32 (2010) 971–978.
[15] C. Keller, M.M. Margulies, Z.H. Hamouche and I. Guillot, Mater. Sci. Eng. A, 527 (2010) 6758–6764.
[16] T. Sakthivel, K. Laha, M. Nandagopal and M.D. Mathew, Mater. High Temp., 31 (2014) 60–68.
[17] M.A. Lebyodkin, N.P. Kobelev, Y. Bougherira, D. Entemeyer, C. Fressengeas, V.S. Gornakov, T.A. Lebedkina and I.V. Shashkov, Acta Mater., 60 (2012) 3729–3740.
[18] H. Aboulfadl, J. Deges, P. Choi and D. Raabe, Acta Mater., 86 (2015) 34–42.
[19] Q.C. Zhang, Z.Y. Jiang, H.F. Jiang, Z.J. Chen and X.P. Wu, Int. J. Plast., 21 (2005) 2150–2173.
[20] K. Kimura, K. Sawada, H. Kushima and K. Kubo, Int. J. Mater. Res., 99 (2008) 395–401.
[21] B.K. Choudhary, E.I. Samuel, G. Sainath, J. Christopher and M.D. Mathew, Metall. Mater. Trans. A, 44 (2013) 4979–4992.
[22] K. Kimura, H. Kushima and K. Sawada, Mater. Sci. Eng. A, 510–511 (2009) 58–63.